Journal: Physical Review Letters
Accession code: LB17853
Article Title: Laser-Driven Proton-Only Acceleration in a Multicomponent Near-Critical-Density Plasma
First Author: Y. Sakawa

AUTHOR QUERIES - TO BE ANSWERED BY THE CORRESPONDING AUTHOR:

The numbered items below correspond to numbers in the margin of the proof pages pinpointing the source of the question and/or comment. The numbers will be removed from the margins prior to publication.

Q: Please check that all references include complete titles.

Q1	Second Proof: Please check and confirm the edit made in author and affiliation group are correct.
Q2	Second Proof: Please note the DOI link in Ref. [25] has been retained as it is.
Q3	Second Proof: Please carefully confirm that all first-proof corrections were addressed and that changes were made accurately.
Q4	Second Proof: Please check and approve that the paper is ready to be published in its current form.

Important Notice to Authors

Attached is a PDF proof of your forthcoming article in PRL. Your article has 6 pages and the Accession Code is LB17853.

Your paper will be in the following section of the journal: LETTERS

No further publication processing will occur until we receive your response to this proof.

All articles, regardless of their original source, are converted into standardized XML, which is then used to create the PDF and online versions of the article as well as to populate third-party systems such as Portico, Crossref, and Web of Science. This process works exceptionally well for most articles; however, please check carefully all key elements of your PDF proof, particularly any equations or tables.

ORCIDs https://orcid.org/

- Follow any ORCID links (iD) after the authors' names and verify that they point to the appropriate record.
- Requests to add ORCIDs should be sent no later than the first proof revisions. If authors do not subsequently add/authenticate ORCIDs within seven business days, production of the paper will proceed and no further requests to add ORCIDs will be processed. See complete details regarding ORCID requests and ORCID verification at https://journals.aps.org/authors/addingorcids-during-proof-corrections.
- If this paper is an Erratum or a Reply, the corresponding author's ORCID may be present if previously provided to APS, but no ORCIDs can be added at proof stage.

Research Organization Registry ID (ROR) https://ror.org/

- Ensure affiliations have been correctly identified by clicking on any institution names that have been linked to the ROR database (blue text). Not all affiliations have an ROR ID, therefore some may not be linked.
- Information about an author's research organization is submitted to Crossref as part of the metadata for articles published by APS.

Crossref Funder Registry ID https://www.crossref.org/services/funder-registry/

- Ensure acknowledgments include all sources of funding for your article, following any requirements of your funding sources. Where possible, please include grant and award ids.
- Information about an article's funding sources is submitted to Crossref to help you comply with funding agency mandates. Crossref's Funder Registry is the definitive registry of funding agencies.

Please carefully check the following funder information we have already extracted from your article and ensure its accuracy and completeness:

- Japan Society for the Promotion of Science, FundRef ID http://dx.doi.org/10.13039/501100001691 (JP/Japan)
- JSPS Core-to-Core Program B. Asia-Africa Science Platforms
- Engineering and Physical Sciences Research Council, FundRef ID http://dx.doi.org/10.13039/501100000266 (GB/United Kingdom of Great Britain and Northern Ireland)

Overall, please proofread the entire formatted article very carefully. The redlined PDF should be used as a guide to see changes that were made during copyediting. However, note that some changes to math and/or layout may not be indicated.

Other Items to Check

- All key elements of the paper, particularly the equations and tabular data. (The original manuscript has been converted to XML prior to the creation of the PDF proof, as described above.)
- Title: It may have changed during the peer-review process.
- Author list: Ensure all names are spelled correctly and all authors are presented in the appropriate order, especially if you have used grouped addresses in REVTeX, which will order authors by institution, not in the order they were entered.
- Contact author: Ensure there is a byline footnote containing the email address for each contact author if desired (Contact author: author@email.com). All emails will be labeled as contact authors to ensure they are picked up by indexing services. A contact author on the published paper does not have to be the corresponding author (see https://journals.aps.org/authors/editorial-policies-authorship#responsibilities.
- Affiliations: Ensure institution names are spelled correctly and attributed to the appropriate author(s). Click on any institution names that have been linked to the ROR database (blue text) to ensure they are correctly identified.
- Receipt date: Please confirm accuracy.
- Acknowledgments: Appropriately acknowledge all funding sources.
- Hyphenation: Please note APS style:
  - Hyphens may have been inserted in word pairs that function as adjectives when they occur before a noun, as in “x-ray diffraction,” “4-mm-long gas cell,” and “R-matrix theory.”
  - Hyphens are deleted from word pairs when they are not used as adjectives before nouns, as in “emission by x rays,” “was 4 mm in length,” and “the R matrix is tested.”
  - Hyphens are not used after prefixes or before suffixes: superresolution, quasiequilibrium, nanoprecipitates, resonancelike, clockwise.
- Figures:
  - Ensure they are accurate and sized properly.
  - Check that all labeling is legible.
  - If you revise any figures, please indicate clearly if any data or results have changed.
  - Figure quality in the proof is representative of the quality to be used in the online journal. Some compression and downsampling of figures may have occurred. Fine details may have become somewhat fuzzy, especially in color figures. The print journal uses higher resolution files and therefore details may be sharper in print.
  - Figures submitted as separate files containing color appear in color on these proofs and in the online journal.
  - For information on color in the print journal see https://journals.aps.org/prl/authors#pubcharges.
- References: Ensure article titles are provided, as appropriate for the journal.
- Supplemental material (SM): Files will not be copyedited or altered by APS after submission and should be submitted in a format ready to be published. You will not receive page proofs of SM. All references cited in SM should be listed in the reference section of the main text. For more information see https://journals.aps.org/authors/supplemental-material-instructions.

Ways to Respond

- ***Web:*** If you accessed this proof online, follow the instructions on the web page to submit corrections.
- ***Email:*** Send corrections to aps-robot@luminad.com. Include the accession code LB17853 in the subject line.

If You Need to Call Us

You may leave a voicemail message at +1.855.808.3897. Please reference the accession code and the first author of your article in your voicemail message. We will respond to you via email.

Laser-Driven Proton-Only Acceleration in a Multicomponent Near-Critical-Density Plasma

Y. Sakawa,[1,*] H. Ishihara,[2] S. N. Ryazantsev,[3,8] M. A. Alkhimova,[3] R. Kumar,[2] O. Kuramoto,[2] Y. Matsumoto,[2] M. Ota,[2,12] S. Egashira,[2] Y. Nakagawa,[2] T. Minami,[4] K. Sakai,[4,12] T. Taguchi,[4] H. Habara,[4] Y. Kuramitsu,[4] A. Morace,[1] Y. Abe,[1,4] Y. Arikawa,[1] S. Fujioka,[1] M. Kanasaki,[5] T. Asai,[5,6] T. Morita,[7] Y. Fukuda,[6] S. Pikuz,[3,8] T. Pikuz,[9] Y. Ohira,[10] L. N. K. Döhl,[11,13] N. Woolsey,[11] and T. Sano[1]

[1]*Institute of Laser Engineering, Osaka University, Suita, Osaka 565-0871, Japan*
[2]*Graduate School of Science, Osaka University, Toyonaka, Osaka 560-0043, Japan*
[3]*Joint Institute for High Temperature, RAS, Moscow 125412, Russia*
[4]*Graduate School of Engineering, Osaka University, Suita, Osaka 565-0871, Japan*
[5]*Graduate School of Maritime Sciences, Kobe University, Kobe 658-0022, Japan*
[6]*Kansai Photon Science Institute (KPSI), National Institutes for Quantum and Radiological Science and Technology (QST), Kizugawa, Kyoto 619-0215, Japan*
[7]*Faculty of Engineering Sciences, Kyushu University, Kasuga, Fukuoka 816-8580, Japan*
[8]*HB11 Energy Holdings, Freshwater, NSW 2095, Australia*
[9]*Institute for Open and Transdisciplinary Research Initiatives, Osaka University, Suita, Osaka, 565-0871 Japan*
[10]*Department of Earth and Planetary Science, The University of Tokyo, Bunkyo-ku, Tokyo 113-0033, Japan*
[11]*York Plasma Institute, School of Physics, Engineering and Technology, University of York, York YO10 5DD, United Kingdom*
[12]*National Institute for Fusion Science, Oroshicho, Toki, Gifu 509-5292, Japan*
[13]*Faculty of Biological Sciences, University of Leeds, Leeds LS2 9JT, United Kingdom*

(Received 8 February 2023; revised 28 May 2024; accepted 5 August 2024)

An experimental investigation of collisionless shock ion acceleration is presented using a multi-component plasma and a high-intensity picosecond duration laser pulse. Protons are the only accelerated ions when a near-critical-density plasma is driven by a laser with a modest normalized vector potential. The results of particle-in-cell simulations imply that collisionless shock may accelerate protons alone selectively, which can be an important tool for understanding the physics of inaccessible collisionless shocks in space and astrophysical plasma.

DOI:

Q1 Collisionless shocks mediated by an ambient magnetic field are ubiquitous in space and astrophysical plasmas and are believed to be sources of high-energy particles or cosmic rays [1–7]. Unmagnetized electrostatic collisionless shocks [8,9] are readily created in laboratory plasmas yet are likely rare phenomena in space [10] and astrophysical systems. However, there are common and important collisionless processes resulting from the reflection and acceleration of particles in the upstream of both magnetized and unmagnetized collisionless shocks, including the excitation of two-stream instabilities [11,12] and shock dissipation by reflected ions [10,12,13]. Therefore, understanding collisionless shocks and the associated particle acceleration processes is of general importance in laboratory experiments and astrophysical systems. Since these processes are difficult to investigate in astrophysical settings due to their remote locations, laboratory experiments are a unique way of studying them. Laser-driven magnetized collisionless shock experiments have been conducted in the last decade [14–20]; because of the large externally applied magnetic field, particle reflection from the magnetized collisionless shock experiments are difficult to observe.

A high-intensity laser-driven plasma can generate a strong electrostatic field, accelerating ions to high energies over short distances. Electrostatic collisionless shock ion acceleration (CSA) [21,22] is one of the laser-driven ion acceleration mechanisms that have been proposed in the last decade [23–25]. In a laser-driven CSA scheme, the ions located ahead of the shock front are reflected at the shock and accelerated to twice the shock velocity by the electrostatic potential at the shock front. By studying reflected and accelerated ions from electrostatic collisionless shocks, such experiments may provide access to plasma processes common to collisionless shocks in general. Furthermore, it might be possible by adjusting the laser and plasma parameters to study the magnetic field generation and amplification mechanisms, such as the Weibel instability [26,27], the Bell [28] and the resonant [29,30] instabilities with a weak external magnetic field, which are predicted to occur in the astrophysical shocks, using the collisionless shock-reflected and accelerated ions.

Various numerical and experimental studies on the CSA mechanism have been carried out [31–43].

*Contact author: sakawa-y@ile.osaka-u.ac.jp

References [32,34] have presented clear experimental evidence for the proton acceleration via the CSA mechanism in a proton plasma using a wavelength of 10-μm laser by measuring a steep electron density profile with the interferometry method when the shock is formed. In the experiments using 0.8 or 1 μm lasers [35–38,40–42], on the other hand, the electron density is hardly measured since the density is too high for the interferometry measurement and assumed to be near or below the critical density ($\sim 10^{21}$ cm^{-3}). Therefore, these works using 0.8- or 1-μm lasers are yet to produce clear signatures demonstrating the generation of a collisionless shock and ion acceleration.

Recently, we demonstrated in two-dimensional (2D) particle-in-cell (PIC) simulations the possibility of producing proton beams in a multicomponent C_2H_3Cl plasma [44–46]. [45] showed two electrostatic collisionless shocks at two distinct longitudinal positions when driven with laser at normalized laser vector potential $a_0 = eE/(m_e \omega c) > 5$ (here e, E, m_e, ω, and c are the electric charge, the laser electric field, the electron mass, angular frequency, and the seed of light, respectively). Moreover, these shocks, associated with protons and carbon (C) ions, accelerate ions to different velocities in an expanding upstream with higher flux than in a single-component hydrogen or C-ion plasma. On the other hand, when $a_0 < 5$, a shock forms only in the proton population. Protons accelerate at this shock, and no C-ion acceleration occurs [44]. This proton-only acceleration in a multicomponent plasma is an important and new feature of the CSA mechanism but has not been demonstrated in the experiment.

In this Letter, we report an experimental investigation of proton-only acceleration in a multicomponent near-critical-density plasma. A high-intensity ps-pulse laser system with a wavelength of 1 μm and $a_0 \simeq 2$ is used as a "drive" laser. A multicomponent near critical density is formed by pre-ablating a thin foil of C_8H_7Cl using an ns-pulse "ablation" laser system before the irradiation of the drive laser. The ion energy spectrum is measured simultaneously with several key electron parameters, such as the density, temperature, and energy spectrum. Without the ablation laser, the measured ion density n_i is close to the solid density n_{solid}, and both protons and carbon ions are accelerated. The proton energy spectrum agrees well with a theoretical model for protons accelerated by the target normal sheath acceleration (TNSA) mechanism [47] using the measured hot-electron temperature. When using an ns-duration laser, a near-critical-density plasma is formed by adjusting the timing and energy. At optimum conditions, only protons are accelerated. Furthermore, the electron density n_e is measured to ensure that these observations were obtained when driving a near critical density ($n_{\mathrm{cr}} = 1.1 \times 10^{21}$ cm^{-3} for a wavelength 1 μm) plasma. The proton spectrum displays more high-energy protons than expected from the TNSA mechanism. The 2D PIC simulations support the measured proton-only acceleration in a multicomponent near-critical-density plasma.

The experiments were performed on LFEX laser at the Institute of Laser Engineering, Osaka University. LFEX delivers up to 210 J/beam of laser energy on target at a wavelength of 1 μm in 1.5 ps with one to three beamlets combined. Spot diameter is about 60 μm, the incidence angle is 21°, the nominal intensity is $(3\text{–}6) \times 10^{18}$ $\mathrm{W/cm^2}$, and $a_0 = 1.6\text{–}2.1$. To generate a near-critical-density plasma with a long scale length on the rear side of the target, a density structure conducive for CSA, the rear surface of the target is irradiated with an ablation laser 2.5 ns before the drive laser. This ablation laser uses one of the Gekko XII beams at a wavelength of 1 μm to deliver approximately 3 J across a 700-μm diameter spot in a 1.3-ns duration pulse. The nominal laser intensity is 3×10^{11} $\mathrm{W/cm^2}$ and the angle of incidence is 32° [48]. The target is a foil of C_8H_7Cl with a thickness of 1 μm.

The plasma density and bulk temperature measurements are conducted with x-ray spectroscopy of highly charged Cl ions using a focusing spectrometer with spatial resolution (FSSR) instrument [49]. FSSR uses a spherically bent crystal (α quartz with Miller indices 101) and provides high spectral resolution ($\lambda/\Delta\lambda \simeq 3000$ for our experimental conditions). FSSR is applied from the rear side of the target and at 42° to the laser axis. Thomson parabola spectrometer (TPS) [50] and electron spectrometer (ESM) located on the axis and 21° from the drive laser beam, respectively, (or 21° and 42°, respectively, from the target normal direction) at the rear side, are used to measure the ion and electron spectra from the rear side of the target. Image plates (IP), BAS-TR2025/Fuji Film, detect FSSR, TPS, and ESM.

Figure 1 shows the experimental (shaded areas) x-ray spectra of highly charged Cl ions using FSSR without [Fig. 1(a)] and with [Fig. 1(b)] the ablation laser. The spectra cover the wavelength of 3.5–4.5 Å. These spectra are normalized to the emission intensity of the Cl Ly_α line (4.185 Å). Solid lines in Fig. 1 represent the modeled x-ray spectra using the collisional-radiative spectral analysis code PrismSPECT [51,52]. For the case without the ablation laser [Fig. 1(a)], the best fit was obtained, assuming that the plasma consists of two zones with different temperatures. The first zone, which represents a hot zone, is determined by the intensities of the lines emitted by H-like ions. First, the intensity ratio of Ly_α and dielectronic satellite lines $\mathrm{Ly}_{\alpha-\mathrm{sat}}/\mathrm{Ly}_\alpha$ is used to adjust the electron temperature T_e. Furthermore, to reproduce the shape of Ly_α, the effect of self-absorption is included by assuming that the plasma is a sphere with a radius R. Finally, the width of all the observed lines is reproduced by adjusting n_i. As a result, plasma parameters of the hot zone are determined as $n_i = (3.2 \pm 0.4) \times 10^{22}$ cm^{-3}, $T_e = 1300 \pm 50$ eV, and $R = 1.0 \pm 0.2$ μm. The second zone, a cold zone, is determined by the intensities of He-like ions, which the

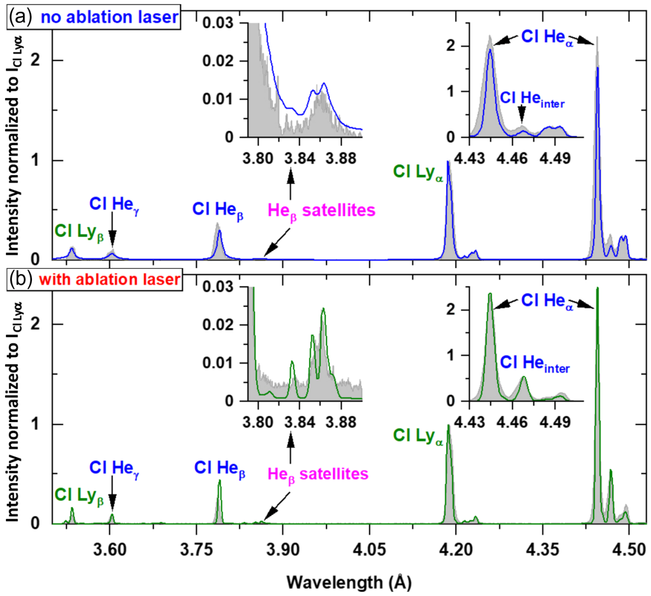

FIG. 1. Comparison of the experimental (shaded areas) and modeled (solid lines) x-ray spectra of highly charged Cl ions from the rear side of C_8H_7Cl target (a) without and (b) with the ablation laser. These spectra are normalized to the emission intensity of the Cl Lyα line (4.185 Å). Insets are expanded spectra of He_β satellites, He_α, and He_{inter}. Matching modeling uses the collisional-radiative spectral analysis code PrismSPECT [51,52]. a_0 is 1.6 and 2.1 for (a) and (b), respectively.

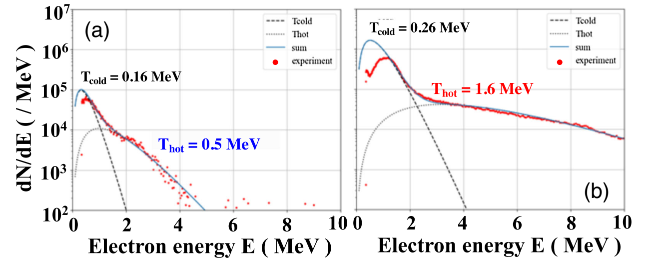

FIG. 2. Derived energy spectra of electrons (red dots) (a) without and (b) with the ablation laser. Two-temperature 3D relativistic Maxwellian distribution [Eq. (1)] is used to fit the measured electron energy spectra. The cold and hot components are displayed with the dotted and broken lines, respectively, and the sum of the two Maxwellian fits is represented by the solid line. The derived temperatures are (a) $T_{cold} = 0.16$ and $T_{hot} = 0.5$ MeV without the ablation laser, and (b) $T_{cold} = 0.26$ and $T_{hot} = 1.6$ MeV with the ablation laser. a_0 is 1.6 and 2.0 for (a) and (b), respectively.

hot zone parameters cannot fit. The intensity ratio of He_α (4.44 Å) and intercombination lines He_{inter}/He_α is used to adjust n_i and T_e, and results in $n_i = (3.2 \pm 0.4) \times 10^{22}$ cm^{-3}, $T_e = 600 \pm 25$ eV, and $R = 1.0 \pm 0.2$ μm. We see that the experimental and modeled x-ray spectra agree with each other. The calculated average charge is $\langle Z \rangle = 4.3$ and the electron density is $n_e = (1.4^{+0.1}_{-0.2}) \times 10^{23}$ cm^{-3}. Note that the measured $n_i = (3.2 \pm 0.4) \times 10^{22}$ cm^{-3} is close to the solid density $n_{solid} = 7.6 \times 10^{22}$ cm^{-3} of C_8H_7Cl target.

For the case with the ablation laser [Fig. 1(b)], nearly 2 orders of magnitude smaller n_i are derived from a significantly higher intensity ratio of He_{inter}/He_α. In this case, the ns ablation laser produces a uniform pre-plasma with small temperature and density gradients. Accordingly, the plasma driven by the ps drive laser is also homogeneous, and a one-zone model is sufficient to describe the results. The intensity ratios of He_{inter} and He_α, and their intensities relative to that of Ly_α are used to adjust n_i and T_e. The self-absorption of the plasma is also included. As a result, $n_i = (3.0 \pm 0.5) \times 10^{20}$ cm^{-3}, and $T_e = 1370 \pm 60$ eV are obtained. In the range of physically reasonable values of $R = 0$–8 μm, the shape of the theoretical spectrum at fixed n_i value depends on weakly on R. Therefore, we do not give the exact value of R, but the theoretical spectrum shown in Fig. 1(b) is obtained for $R = 0.25$ μm. The modeled x-ray spectrum is shown by the solid line in Fig. 1(b) and agrees well with that obtained from the experiment. The calculated average charge $\langle Z \rangle = 4.3$ and the electron density $n_e = (1.3 \pm 0.2) \times 10^{21}$ cm^{-3}. The measured n_e is close to the critical density $n_{cr} = 1.1 \times 10^{21}$ cm^{-3}, and we confirmed that a suitable plasma condition for CSA is achieved when using an ablation laser.

Figure 2 shows the electron energy spectrum (red dots) obtained from ESM without [Fig. 2(a)] and with [Fig. 2(b)] the ablation laser. To derive the electron temperature, we use the following two-temperature 3D relativistic Maxwellian distribution,

$$\frac{dN}{dE} = c_{cold} E^2 \exp\left(-\frac{E}{T_{cold}}\right) + c_{hot} E^2 \exp\left(-\frac{E}{T_{hot}}\right). \quad (1)$$

Here, N and E are, respectively, the number and energy of the electrons, c_{cold} (c_{hot}) and T_{cold} (T_{hot}) are a scaling factor and the electron temperature for the cold (hot) component, respectively. In Fig. 2, fitted functions of the cold and hot components are displayed with dotted and broken lines, respectively, and the sum of the two Maxwellian fits is represented by a solid line. The two-temperature approximation reproduces the measured electron spectrum in the $E > 1$ MeV energy range. The shifts in the peak energy of the cold components result from the plasma potential at the target's rear side. The T_e derived from FSSR is roughly 2 orders smaller than T_{cold}. This is because FSSR measures the temperature of electrons within the bulk plasma, while the ESM measures electrons with energies sufficient to leave the plasma.

Figures 3(a) and 3(b) display raw data of TPS without and with the ablation laser, respectively. We fit the parabola signals with the least squares fitting method [50]. An infinite energy point is determined from the dot on the left side of the IP. Background signals are taken from the trajectory at 10 pixels from each signal. Signals from protons and carbon ions appear when the drive laser alone

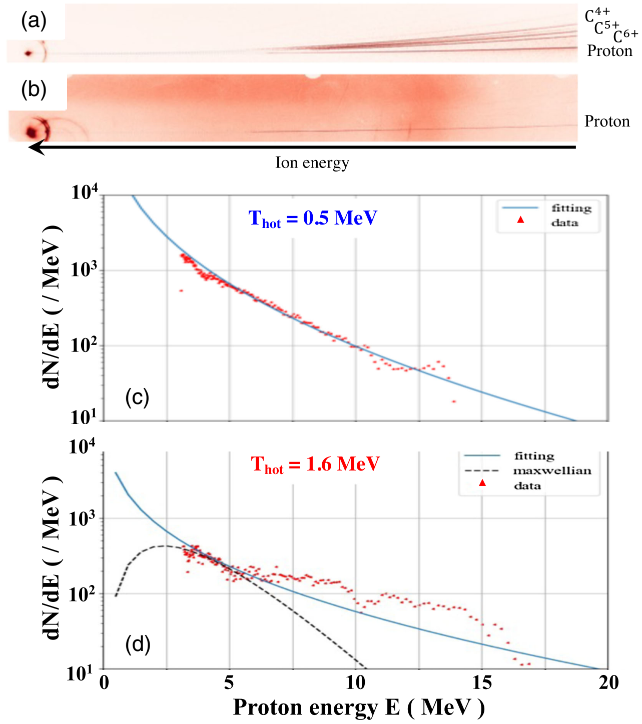

FIG. 3. Raw data of TPS (a) without and (b) with the ablation laser. a_0 is 1.6 and 2.0 for (a) and (b), respectively. Derived energy spectra of protons (red dots) (c) without and (d) with the ablation laser. The error bars or standard deviations in the y-axis in (d) are less than 1% in the energy ranges of $E = 6$–15 MeV. Theoretical energy spectra of protons accelerated by the TNSA mechanism [Eq. (2)] (solid lines) are shown in (c) and (d) for the measured hot-electron temperatures of $T_{\mathrm{hot}} = 0.5$ and 1.6 MeV, respectively. The dashed line in (d) fits the Maxwellian proton distribution.

is used, but only a proton signal is detected when the ablation laser is used.

Figures 3(c) and 3(d) present inferred energy spectra of protons (red dots) without and with the ablation laser, respectively. Reference [47] has derived a theoretical energy spectrum for the ions accelerated by the TNSA mechanism using a hot-electron temperature (T_{hot}) as follows,

$$\frac{dN}{dE} = \frac{c_{\mathrm{ion}}}{\sqrt{ET_{\mathrm{hot}}}} \exp\left(-\sqrt{\frac{E}{T_{\mathrm{hot}}}}\right), \tag{2}$$

where N and E are the number and energy of the protons, and c_{ion} is a scaling factor. We adjust c_{ion} so that Eq. (2) fits the measured spectra. For the no-ablation-laser case [Fig. 3(c)], the measured ion spectrum is in good agreement with the TNSA model (the solid line) with the measured electron temperature $T_{\mathrm{hot}} = 0.5$ MeV. On the other hand, with the ablation laser [Fig. 3(d)], the theoretical energy spectrum of the TNSA protons using the measured $T_{\mathrm{hot}} =$ 1.6 MeV (the solid line) fits the measured spectrum only

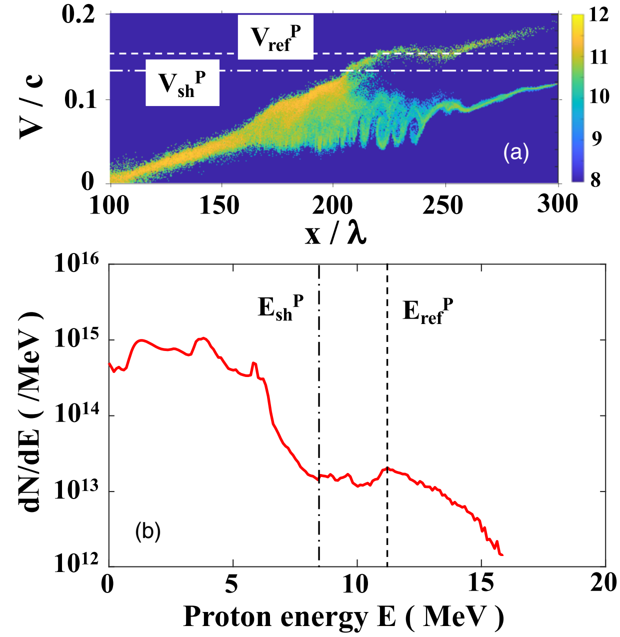

FIG. 4. 2D PIC simulation results for a C_8H_7Cl plasma at $a_0 = 2.1$ and $t = 6.75$ ps. (a) Phase space of protons and (b) energy spectra of the protons taken with $v_x > 0$. The color scale shows the number of protons on a log scale. The velocities (energies) of the shock $V_{\mathrm{sh}}^{\mathrm{P}}$ ($E_{\mathrm{sh}}^{\mathrm{P}}$) and the reflected protons $V_{\mathrm{ref}}^{\mathrm{P}}$ ($E_{\mathrm{ref}}^{\mathrm{P}}$) are shown in the dash-dotted and dotted lines, respectively.

around the proton energy of $E = 2.6$–6.0 MeV, and above $E \simeq 6.0$ MeV, the number of the accelerated protons is larger than the TNSA model. The dashed line in Fig. 3(d) is the Maxwellian distribution. These results suggest that when the ablation laser is used and the plasma density is near critical, some mechanisms other than TNSA contribute to ion acceleration.

To identify the mechanism of the proton-only acceleration, we examine numerical simulations of CSA in a multicomponent C_8H_7Cl plasma, using the 2D PIC simulation code EPOCH [53]. The laser parameters are $a_0 = 2.1$ and a Gaussian temporal profile with 1.5 ps full-width-at-half-maximum, and the maximum electron density is the relativistic critical density $a_0 n_{cr}$ [44–46]. Details of the simulations, including the target density profiles, are given in [44].

Figures 4(a) and 4(b) represent the proton phase space and the energy spectrum taken with $v_x > 0$, respectively. The velocities (energies) of the shock $V_{\mathrm{sh}}^{\mathrm{P}}$ ($E_{\mathrm{sh}}^{\mathrm{P}}$) and the reflected protons $V_{\mathrm{ref}}^{\mathrm{P}}$ ($E_{\mathrm{ref}}^{\mathrm{P}}$) are shown in the dash-dotted and dotted lines, respectively. A significant population of protons satisfies the condition for CSA, $v_L^i \le v_0^i \le V_{\mathrm{sh}}^i$ [44–46,54], where v_0^i is the drift velocity of the upstream ions, $v_L^i = V_{\mathrm{sh}}^i - \sqrt{2(Z_i/A_i)e\phi/m_p}$ is the lower-threshold velocity, Z_i and A_i are the ionic charge and mass numbers, respectively, e is the electric charge, ϕ is the electrostatic potential at the shock front, m_p is the proton mass, the higher-threshold velocity $V_{\rm sh}^{i}$ is the shock velocity, and i represents the different ion species ($i = \mathrm{P}$ and C for protons and C^{6+} ions, respectively). As a result, protons in the upstream region are reflected and accelerated at the collisionless shock [44–46]. However, no C^{6+} ions are reflected by this collisionless shock, as this requires $V_{\rm sh}^{\rm C} = V_{\rm sh}^{\rm P}$ since the velocities of upstream C^{6+} ions are lower than $v_L^{\rm C}$. Furthermore, the carbon-ion Mach number [45] $M^{\rm C} < 1$ for $a_0 = 2.1$, and no shock is associated with C^{6+} ions. Furthermore, the maximum proton energies obtained from the experiment [Fig. 3(d)] and PIC [Fig. 4(b)] agree very well with each other. Therefore, proton-only acceleration may occur via the CSA mechanism.

The authors of [55] have measured the TNSA-proton energy spectra as a function of the scale lengths of the rear-side plasma ($l_{\rm rear}$) by changing the timing of the second high-intensity laser-beam irradiation on the rear side of the target from the drive laser beam. Without the second laser beam or when $l_{\rm rear} = 0$, the maximum proton energy was $\simeq$13.5 MeV. When $l_{\rm rear} = 9.2$ μm, the maximum proton energy decreased to $\simeq$7.5 MeV. Note that the proton spectrum up to the proton energy of $\simeq$6 MeV was nearly identical for both cases. Therefore, in their experiment, the maximum density is close to solid density. Protons are accelerated by TNSA, and the maximum proton energy decreases when the second laser is used because of a reduced rear-side sheath electric field [55]. Our case differs from [55], as the ablation laser duration is long and the $n_e \simeq n_{\rm cr}$. We observe a number of protons larger than that predicted for TNSA. As calculated by the 2D PIC simulation, CSA can accelerate only protons at $a_0 \simeq 2$. We suggest this experiment isolates the CSA and that this is the only mechanism accelerating ions, and in this case, only protons. We have used a multicomponent (protons and C^{6+} ions) in a near-critical-density plasma at $a_0 \simeq 2$.

In summary, we investigated collisionless shock ion acceleration (CSA) using a high-intensity ps-pulse laser system with a modest normalized vector potential. In a near-critical-density plasma containing the multicomponent ion species C_8H_7Cl, only protons are accelerated.

In a near-critical-density multicomponent proton and C^{6+}-ion plasma, 2D PIC calculations suggest that it might be possible to control accelerated ions actively (proton-only or proton and C^{6+}-ion acceleration) by changing the drive-laser intensity in CSA. The collisionless shock-reflected and accelerated ions are essential in the Galactic cosmic ray generation via diffusive shock acceleration [56–58], and the magnetic field generation and amplification via instabilities [26–30]. This work illustrates how laboratory studies of ion acceleration at collisionless shocks can be an important tool for understanding some collisionless physics associated with space and astrophysical shocks.

Acknowledgments—This research was partially supported by the Japan Society for the Promotion of Science (JSPS) KAKENHI Grants No. JP15H02154, No. JP17H06202, No. JP19H00668, No. JP19H01893, No. JP22H00119, JSPS Core-to-Core Program B. Asia-Africa Science Platforms Grant No. JPJSCCB20190003, and UK EPSRC Grants No. EP/L01663X/1 and No. EP/P026796/1.

[1] R. Z. Sagdeev, Cooperative phenomena and shock waves in collisionless plasmas, Rev. Plasma Phys. **4**, 23 (1966).
[2] A. R. Bell, Mon. Not. R. Astron. Soc. **182**, 147 (1978).
[3] R. D. Blandford and J. P. Ostriker, Astrophys. J. **221**, L29 (1978).
[4] C. S. Wu, J. Geophys. Res. **89**, 8857 (1984).
[5] L. Ball and D. B. Melrose, Pub. Astron. Soc. Aust. **18**, 361 (2001).
[6] M. Hoshino, Prog. Theor. Phys. Suppl. **143**, 149 (2001).
[7] Y. Sakawa, T. Morita, Y. Kuramitsu, and H. Takabe, Adv. Phys. **1**, 425 (2016).
[8] D. Forslund and C. Shonk, Phys. Rev. Lett. **25**, 281 (1970).
[9] D. W. Forslund, R. L. Morse, and C. W. Nielson, Phys. Rev. Lett. **27**, 1424 (1971).
[10] A. Balogh and R. A. Treumann, *Physics of Collisionless Shocks: Space Plasma Shock Waves* (Springer Science & Business Media, New York, 2013).
[11] Y. Ohira and F. Takahara, Astrophys. J. **688**, 320 (2008).
[12] R. A. Treumann, Astron. Astrophys. Rev. **17**, 409 (2009).
[13] H. Madanian, S. J. Schwartz, J. S. Halekas, and L. B. Wilson, Geophys. Res. Lett. **47**, 1 (2020).
[14] N. C. Woolsey, Y. A. Ali, R. G. Evans, R. a. D. Grundy, S. J. Pestehe, P. G. Carolan, N. J. Conway, R. O. Dendy, P. Helander, K. G. McClements, J. G. Kirk, P. a. Norreys, M. M. Notley, and S. J. Rose, Phys. Plasmas **8**, 2439 (2001).
[15] C. Niemann, W. Gekelman, C. G. Constantin, E. T. Everson, D. B. Schaeffer, A. S. Bondarenko, S. E. Clark, D. Winske, S. Vincena, B. Van Compernolle, and P. Pribyl, Geophys. Res. Lett. **41**, 7413 (2014).
[16] D. B. Schaeffer, W. Fox, D. Haberberger, G. Fiksel, A. Bhattacharjee, D. H. Barnak, S. X. Hu, and K. Germaschewski, Phys. Rev. Lett. **119**, 025001 (2017).
[17] D. B. Schaeffer, W. Fox, R. K. Follett, G. Fiksel, C. K. Li, J. Matteucci, A. Bhattacharjee, and K. Germaschewski, Phys. Rev. Lett. **122**, 245001 (2019).
[18] W. Yao *et al.*, Nat. Phys. **17**, 1177 (2021).
[19] R. Yamazaki *et al.*, Phys. Rev. E **105**, 025203 (2022).
[20] S. Matsukiyo *et al.*, Phys. Rev. E **106**, 025205 (2022).
[21] J. Denavit, Phys. Rev. Lett. **69**, 3052 (1992).
[22] L. O. Silva, M. Marti, J. R. Davies, R. A. Fonseca, C. Ren, F. Tsung, and W. B. Mori, Phys. Rev. Lett. **92**, 015002 (2004).
[23] H. Daido, M. Nishiuchi, and A. S. Pirozhkov, Rep. Prog. Phys. **75**, 056401 (2012).
[24] A. Macchi, M. Borghesi, and M. Passoni, Rev. Mod. Phys. **85**, 751 (2013).
[25] S. V. Bulanov, J. J. Wilkens, T. Z. Esirkepov, G. Korn, G. Kraft, S. D. Kraft, M. Molls, and V. Khoroshkov, Phys. Usp. **57**, 1149 (2014). Q2
[26] E. Weibel, Phys. Rev. Lett. **2**, 83 (1959).
[27] B. D. Fried, Phys. Fluids **2**, 10 (1959).

[28] A. R. Bell, Mon. Not. R. Astron. Soc. **353**, 550 (2004).

[29] R. Kulsrund and W. P. Pearce, Astrophys. J. **156**, 445 (1969).

[30] D. G. Wentzel, Annu. Rev. Astron. Astrophys. **12**, 71 (1974).

[31] A. Macchi, A. S. Nindrayog, and F. Pegoraro, Phys. Rev. E **85**, 046402 (2012).

[32] D. Haberberger, S. Tochitsky, F. Fiuza, C. Gong, R. A. Fonseca, L. O. Silva, W. B. Mori, and C. Joshi, Nat. Phys. **8**, 95 (2012).

[33] F. Fiuza, A. Stockem, E. Boella, R. A. Fonseca, L. O. Silva, D. Haberberger, S. Tochitsky, C. Gong, W. B. Mori, and C. Joshi, Phys. Rev. Lett. **109**, 215001 (2012).

[34] O. Tresca, N. P. Dover, N. Cook, C. Maharjan, M. N. Polyanskiy, Z. Najmudin, P. Shkolnikov, and I. Pogorelsky, Phys. Rev. Lett. **115**, 094802 (2015).

[35] P. Antici, E. Boella, S. N. Chen, D. S. Andrews, M. Barberio, J. Böker, F. Cardelli, J. L. Feugeas, M. Glesser, P. Nicolaï, L. Romagnani, M. Scisciò, M. Starodubtsev, O. Willi, J. C. Kieffer, V. Tikhonchuk, H. Pépin, L. O. Silva, E. D. Humières, and J. Fuchs, Sci. Rep. **7**, 16463 (2017).

[36] H. Zhang, B. F. Shen, W. P. Wang, S. H. Zhai, S. S. Li, X. M. Lu, J. F. Li, R. J. Xu, X. L. Wang, X. Y. Liang, Y. X. Leng, R. X. Li, and Z. Z. Xu, Phys. Rev. Lett. **119**, 164801 (2017).

[37] S. N. Chen, M. Vranic, T. Gangolf, E. Boella, P. Antici, M. Bailly-Grandvaux, P. Loiseau, H. Pépin, G. Revet, J. J. Santos, A. M. Schroer, M. Starodubtsev, O. Willi, L. O. Silva, E. D'humières, and J. Fuchs, Sci. Rep. **7**, 13050 (2017).

[38] A. Pak, S. Kerr, N. Lemos, A. Link, P. Patel, F. Albert, L. Divol, B. B. Pollock, D. Haberberger, D. Froula, M. Gauthier, S. H. Glenzer, A. Longman, L. Manzoor, R. Fedosejevs, S. Tochitsky, C. Joshi, and F. Fiuza, Phys. Rev. Accel. Beams **21**, 103401 (2018).

[39] R. Matsui, Y. Fukuda, and Y. Kishimoto, Phys. Rev. Lett. **122**, 014804 (2019).

[40] M. Ota, A. Morace, R. Kumar, S. Kambayashi, S. Egashira, M. Kanasaki, Y. Fukuda, and Y. Sakawa, High Energy Density Phys. **33**, 100697 (2019).

[41] P. K. Singh, V. B. Pathak, J. H. Shin, I. W. Choi, K. Nakajima, S. K. Lee, J. H. Sung, H. W. Lee, Y. J. Rhee, C. Aniculaesei, C. M. Kim, K. H. Pae, M. H. Cho, C. Hojbota, S. G. Lee, F. Mollica, V. Malka, C. M. Ryu, H. T. Kim, and C. H. Nam, Sci. Rep. **10**, 18452 (2020).

[42] S. Tochitsky, A. Pak, F. Fiuza, D. Haberberger, N. Lemos, A. Link, D. H. Froula, and C. Joshi, Phys. Plasmas **27**, 083102 (2020).

[43] E. Boella, R. Bingham, R. A. Cairns, P. Norreys, R. Trines, R. Scott, M. Vranic, N. Shukla, and L. O. Silva, Phil. Trans. R. Soc. A **379**, 20200039 (2021).

[44] R. Kumar, Y. Sakawa, L. N. K. Döhl, N. Woolsey, and A. Morace, Phys. Rev. Accel. Beams **22**, 043401 (2019).

[45] R. Kumar, Y. Sakawa, T. Sano, L. N. K. Döhl, N. Woolsey, and A. Morace, Phys. Rev. E **103**, 043201 (2021).

[46] Y. Sakawa, Y. Ohira, R. Kumar, A. Morace, L. N. K. Döhl, and N. Woolsey, Phys. Rev. E **104**, 055202 (2021).

[47] P. Mora, Phys. Rev. Lett. **90**, 185002 (2003).

[48] See Supplemental Material at http://link.aps.org/supplemental/10.1103/PhysRevLett.000.000000 for additional data.

[49] A. Y. Faenov, S. A. Pikuz, A. I. Erko, B. A. Bryunetkin, V. M. Dyakin, G. V. Ivanenkov, A. R. Mingaleev, T. A. Pikuz, V. M. Romanova, and T. A. Shelkovenko, Phys. Scr. **50**, 333 (1994).

[50] Y. Kuramitsu *et al.*, Sci. Rep. **12**, 2346 (2022).

[51] https://www.prism-cs.com/Software/PrismSPECT.html.

[52] J. J. MacFarlane, I. E. Golovkin, P. R. Woodruff, D. R. Welch, B. V. Oliver, T. A. Mehlhorn, and R. B. Campbell, *Inertial Fusion Sciences and Applications 2003: State of the Art*, edited by B. A. Hammel, D. D. Meyerhofer, J. Meyer-terVehn, and H. Azechi (American Nuclear Society, La Grange Park, IL, 2004), p. 457.

[53] T. D. Arber, K. Bennett, C. S. Brady, A. Lawrence-Douglas, M. G. Ramsay, N. J. Sircombe, P. Gillies, R. G. Evans, H. Schmitz, A. R. Bell, and C. P. Ridgers, Plasma Phys. Controlled Fusion **57**, 113001 (2015).

[54] D. A. Tidman and N. A. Krall, *Shock Waves in Collisionless Plasmas* (Wiley-Interscience, New York, 1971).

[55] J. Fuchs, C. A. Cecchetti, M. Borghesi, T. Grismayer, E. d'Humières, P. Antici, S. Atzeni, P. Mora, A. Pipahl, L. Romagnani, A. Schiavi, Y. Sentoku, T. Toncian, P. Audebert, and O. Willi, Phys. Rev. Lett. **99**, 015002 (2007).

[56] D. Caprioli, D. T. Yi, and A. Spitkovsky, Phys. Rev. Lett. **119**, 171101 (2017).

[57] D. Caprioli, A. R. Pop, and A. Spitkovsky, Astrophys. J. Lett. **798**, L28 (2015). **Q3**

[58] Y. Ohira, N. Kawanaka, and K. Ioka, Phys. Rev. D **93**, 083001 (2016). **Q4**